Structure of human argininosuccinate synthetase

Tobias Karlberg, Ruairi Collins, Susanne van den Berg, Alex Flores, Martin Hammarström, Martin Högbom,‡ Lovisa Holmberg Schiavone and Jonas Uppenberg*

Structural Genomics Consortium, Karolinska Institutet, MBB/SGC, 171 77 Stockholm, Sweden

‡ Current address: Center for Biomembrane Research, Department of Biochemistry and Biophysics, Stockholm University, Sweden.

Correspondence e-mail: jonas.uppenberg@yahoo.se

Argininosuccinate synthetase catalyzes the transformation of citrulline and aspartate into argininosuccinate and pyrophosphate using the hydrolysis of ATP to AMP and pyrophosphate. This enzymatic process constitutes the rate-limiting step in both the urea and arginine–citrulline cycles. Previous studies have investigated the crystal structures of argininosuccinate synthetase from bacterial species. In this work, the first crystal structure of human argininosuccinate synthetase in complex with the substrates citrulline and aspartate is presented. The human enzyme is compared with structures of argininosuccinate synthetase from bacteria. In addition, the structure also provides new insights into the function of the numerous clinical mutations identified in patients with type I citrullinaemia (also known as classic citrullinaemia).

1. Introduction

Argininosuccinate synthetase (ASS; EC 6.3.4.5; citrulline–aspartate ligase) is the rate-limiting enzyme in the synthesis of the amino acid arginine (Ratner & Petrack, 1951; Schimke, 1964). In humans, the final steps of arginine synthesis are part of the urea cycle, which is responsible for the detoxification of ammonia by its conversion into urea. In the forward reaction of ASS, citrulline, aspartate and ATP are substrates in the production of argininosuccinate, pyrophosphate and AMP (reviewed in Husson *et al.*, 2003).

In mammals, the urea-cycle enzymes ASS and argininosuccinate lyase are part of an additional pathway together with the enzyme nitric oxide synthase (NOS), forming the arginine–citrulline cycle. This pathway ensures the supply of nitric oxide, which plays many roles as a signalling molecule in mammalian processes, such as immune defence and vascular regulation (Mori & Gotoh, 2000). In humans ASS activity has been shown to be down-regulated by NOS through nitrosylation of a specific cysteine residue (Hao *et al.*, 2004).

Type I citrullinaemia is a disorder caused by mutations in the ASS gene leading to reduced or abolished activity of the ASS enzyme (McMurray *et al.*, 1962). The disease is characterized by accumulation in the bloodstream of ammonia and other byproducts of the urea cycle. A large number of mutations in the human ASS (hASS) gene (Gao *et al.*, 2003; Häberle *et al.*, 2003) have been identified in patients and for some of these a potential structural role has been proposed from the existing structures of ASS from bacteria (Lemke & Howell, 2001). From the solved crystal structure of hASS presented in this study, we have reassessed and expanded on the suggested structural roles.

research papers

Table 1
Data-collection and refinement statistics.

Values in parentheses are for the highest resolution shell.

Data collection	
Beamline	ID 14.1
Wavelength (Å)	0.95373
Space group	$F222$
Unit-cell parameters (Å, °)	$a = 95.94$, $b = 117.47$, $c = 155.15$, $\alpha = \beta = \gamma = 90$
Resolution (Å)	30–2.4 (2.5–2.4)
No. of reflections	17358 (1967)
R_{merge} (%)	15.2 (45.5)
Completeness (%)	99.7 (100)
Redundancy	7.3 (7.5)
$\langle I \rangle / \langle \sigma(I) \rangle$	8.6 (4.0)
Refinement	
Resolution (Å)	19.4–2.4 (2.5–2.4)
R factor (%)	19.8 (19.1)
Reflections used for R factor	16407
R_{free} (%)	26.5 (25.9)
Reflections used for R_{free}	864
R.m.s.d. bond lengths† (Å)	0.014
R.m.s.d. bond angles† (°)	1.86
No. of atoms in model	
All atoms	3423
Protein atoms	3191
Solvent atoms	210
Ligand atoms	22
Average B factors (Å^2)	
All atoms	18.0
Protein atoms	18.0
Solvent atoms	18.6
Ligand atoms	17.3
DPI coordinate error	0.2546
Ramachandran plot‡	
Most favoured (%)	89.3
Disallowed (%)	0

† Using the parameters of Engh & Huber (1991).   ‡ Calculated using *PROCHECK* (Laskowski *et al.*, 1993).

The crystal structures of argininosuccinate synthetase from two bacterial species, *Escherichia coli* (Lemke & Howell, 2001, 2002) and *Thermus* (*Tm.*) *thermophilus* (Goto *et al.*, 2002, 2003), have previously been reported. In addition, one unpublished apo structure from the bacterium *Thermotoga* (*Tt.*) *maritima* was found in the Protein Data Bank (PDB code 1vl2). The structures of ASS from bacteria cover many different combinations of substrate, substrate analogue and product. For the *E. coli* enzyme (ecASS), complexes with the following ligands are available: with ATP, with aspartate and citrulline and with citrulline and ATP. For *Tm. thermophilus* ASS (ttASS) complexes with ATP, with succinate, arginine and AMP-PNP (an ATP analogue), with AMP and argininosuccinate and with citrulline, aspartate and ATP are available. The oligomeric arrangement of ASS as a tetramer is strictly conserved between the bacterial species. In the cases of *Tm. thermophilus* and *Tt. maritima* (tmASS) the tetramer constitutes the asymmetric unit, whereas in *E. coli* the tetramer is generated by crystal symmetry from a monomer in the asymmetric unit.

hASS shares an amino-acid sequence identity of 29, 53 and 59% with the determined *E. coli*, *Tm. thermophilus* and *Tt. maritima* structures, respectively. In this study, we report the crystal structure of hASS in complex with the substrate molecules citrulline and aspartate.

2. Material and methods

2.1. Cloning, protein expression and purification

The coding region (residues 1–412) of the human argininosuccinate synthetase gene (GenBank accession No. X01630; Swiss-Prot name ASSY_HUMAN) was cloned by ligation-independent cloning into a pET-28-based expression vector incorporating a TEV-cleavable N-terminal His-tag fusion (pNIC-Bsa4, sequence MHHHHHHSSGVDLGTEN-LYFQS). After transformation and liquid-culture growth in Terrific Broth using standard methods, recombinant expression of hASS was induced at 291 K by the addition of 0.5 mM isopropyl β-D-1-thiogalactopyranoside. After harvesting, the cell pellets were suspended in IMAC (immobilized metal-ion affinity chromatography) binding buffer supplemented with protease inhibitor and stored at 193 K. hASS was purified using IMAC on a His-Trap Crude column, followed by gel filtration on a Superdex 200 column (columns from GE Healthcare, Uppsala, Sweden). IMAC binding buffer contained 50 mM sodium phosphate, 10%(v/v) glycerol, 0.5 mM TCEP, 300 mM NaCl, 10 mM imidazole pH 7.5. IMAC elution buffer was identical except that the imidazole concentration was raised to 500 mM. TEV protease was added to a final concentration of 1.3 μM and incubated at 277 K for 16 h. The cleaved histidine tag was removed using a His-Trap column, leaving a serine residue at the N-terminal end of the protein sequence. The protein was concentrated and the buffer was exchanged using an Amicon ultrafilter. The buffer solution contained 500 mM NaCl, 2 mM TCEP and 30 mM HEPES pH 7.5. The final protein concentration was 32 mg ml^{-1}.

2.2. Crystallization

The crystallization conditions for hASS were initially identified from the 96 conditions of the JCSG (Joint Center for Structural Genomics) crystal screen (condition No. 80; Page *et al.*, 2003). Optimized crystals were produced at room temperature with the hanging-drop method using a drop containing 1 μl protein solution and 1 μl reservoir solution. The protein solution contained 17 mg ml^{-1} protein, 10 mM aspartate and 10 mM citrulline. The reservoir solution contained 16%(w/v) PEG 3350, 0.15 M DL-malic acid pH 7.0. Microseeding with crystals from the initial screen was performed 1 d after experiment setup.

2.3. Data collection

Crystals were transferred to a cryoprotectant consisting of a modified crystallization reservoir solution containing 24%(v/v) glycerol. A data set extending to 2.4 Å resolution was collected at 0.95373 Å wavelength on a MAR CCD detector at beamline 14.1 at BESSY II (Berlin, Germany). The data were integrated and scaled using *XDS* (Kabsch, 1993). The crystals belonged to space group $F222$ and the Matthews coefficient suggested the presence of one monomer in the asymmetric unit. Crystallographic statistics are summarized in Table 1.

2.4. Structure solution

The structure was solved by molecular replacement using *MOLREP* (Vagin & Teplyakov, 1997). The structure of bacterial argininosuccinate synthetase from *Tt. maritima* was used as a search model (PDB code 1vl2). A single molecule was found in the asymmetric unit. One molecule of hASS was built into the electron density with *Coot* (Emsley & Cowtan, 2004), using the search model as template. After initial refinement, water molecules were added with the *Coot* 'find waters' algorithm. Substrate ligands were modelled into density, guided by the *Tm. thermophilus* structure 1j1z containing aspartate and citrulline. The model was refined with *REFMAC*5 (Murshudov *et al.*, 1997). In the refinement, data in the 19.4–2.4 Å resolution interval were used and the progress of refinement was followed from the decreasing R and R_{free} values.

2.5. Modelling of ATP

An ATP molecule was superposed on the hASS structure by alignment of the nucleotide-binding domain (residues 4–63 and 99–147) from ttASS (complex with ATP, citrulline and aspartate; PDB code 1j1z). The 108 aligned C^{α} atoms from the two proteins had an r.m.s.d. of 0.74 Å.

2.6. Modelling of nitrosocysteine

The PDB was searched for protein structures containing cysteine residues modified by covalent nitrosylation. Five modified residues were found in three unique structures: blackfin tuna myoglobin (PDB code 2nrm; Schreiter *et al.*, 2007), human thioredoxin (2ifq; Weichsel *et al.*, 2007) and human haemoglobin (1buw; Chan *et al.*, 1998). These residues were aligned with respect to the C^{α}, C^{β} and S^{γ} atoms of hASS Cys132 using *Coot*.

2.7. Structural comparisons

The program *LSQMAN* (Kleywegt, 1999) was used for r.m.s.d. calculations, using the fast alignment algorithm with default settings.

3. Results and discussion

3.1. Overall structure

We have determined the crystal structure of hASS in complex with citrulline and aspartate. The protein crystallizes with one monomer in the asymmetric unit and the functional tetramer, which consists of two identical dimers, was generated by the crystallographic symmetry operators.

The structure of hASS consists of three domains: a nucleotide-binding domain, a synthetase domain and a C-terminal helix involved in oligomerization. The two first domains are highly integrated, with two connected helices from the nucleotide-binding domain running through the core of the synthetase domain.

The complete human protein of 412 residues was crystallized. The final structure contains residues 4–407, with the

exceptions of the surface-loop residues 156 and 377, for which no density could be observed. A larger portion of the loop connecting the core protein to the C-terminal helix can be observed compared with previously published structures.

The overall structure of hASS is highly similar to the bacterial structures. This similarity spans both the nucleotide and synthetase domains, as well as the C-terminal helix. The tetrameric arrangement is also highly conserved between the bacterial and human structures.

A structure-based sequence alignment of hASS with the other ASS structures reveals a few insertions and deletions (Fig. 1). Relative to ecASS, structure deletions occur at the following positions in the human structure (the size of deletion, if more than one residue, is given in parentheses): Gln40 (2), Asp85 (3), Glu196 (2), Lys340, Gly362 and Gly381. Relative to ttASS, one deletion is found at residue Gln27. Likewise, a few insertions exist in the human structure, the most prominent being an extended β-hairpin at residues Asn237–Gly241 compared with ttASS and ecASS. Another insertion is folded as an α-helix relative to ttASS and is found between residues 147 and 153. Both of these insertions are exposed to the surface and are not involved in the packing of the two domains.

An overall structural comparison of hASS with the bacterial structures showed the highest similarity to tmASS; the r.m.s.d. for C^{α} atoms was 1.03 Å with 385 residues aligned. For ttASS the corresponding values were in the ranges 1.01–1.12 Å and 368–376 residues, respectively, for the six published structures (molecule *A* from ttASS was used in all cases). For ecASS a distinct difference was observed between the structures with and without the presence of ATP. For the two structures with no ATP present (PDB codes 1k92 and 1k97) the values were 1.61 Å over 346 residues and 1.61 Å over 343 residues, respectively. With ATP present (PDB codes 1kp2 and 1kp3) these values were 1.4 Å over 299 residues and 1.46 Å over 318 residues, respectively. This is in agreement with the observation of a conformational change in ecASS on binding of ATP. When the individual domains are compared with the human structure, the difference from ecASS is most pronounced for the synthetase domain, with an r.m.s.d. of 2.29 Å with no ATP present (1k92) and 2.25 Å with ATP (1kp2). The values for the corresponding nucleotide domain are 1.43 Å and 1.32 Å, respectively. In contrast, no great difference between the domains is seen on comparison with ttASS; the r.m.s.d. is 0.85 Å for the nucleotide domain and 0.89 Å for the synthetase domain (1j1z).

The hASS tetrameric complex was also structurally aligned with earlier structures with an r.m.s.d. of 1.54 Å over 1352 residues to tmASS (1vl2), 1.49 Å over 1445 residues to ttASS (1kh1) and 1.95 Å over 1119 residues to ecASS (1k97).

3.2. Dimer interface

The main interface between monomers in ASS is formed exclusively between two synthetase domains related by a twofold rotation. This interface is made up of helices 10 and 11, strands 11 and 14, a β-hairpin at residues 84–87 and an
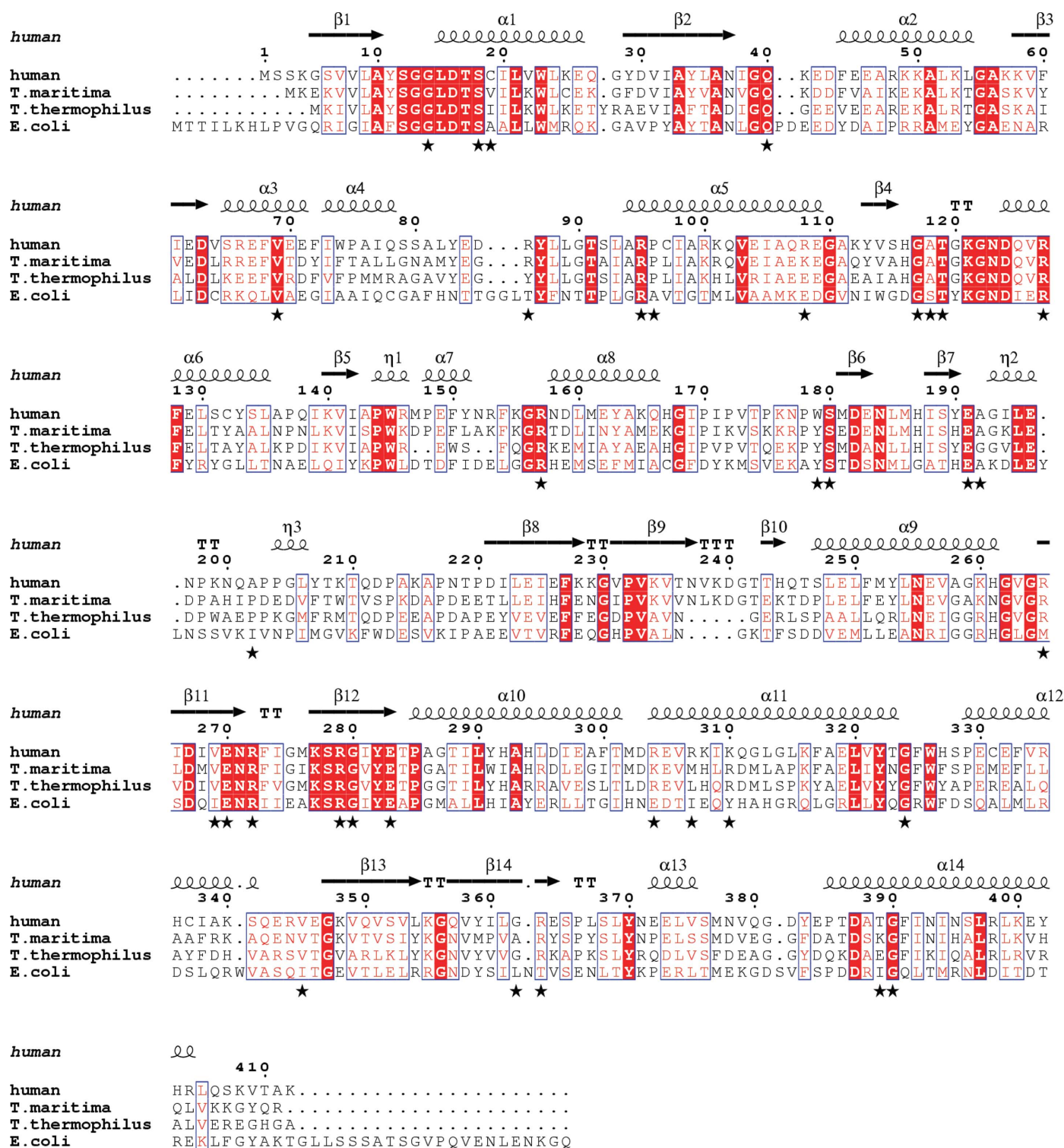
Figure 1
Sequence alignment of argininosuccinate synthetases from human and bacterial sources for which three-dimensional structures are available. The residues for which clinical mutations have been identified in the human sequence are marked with a star. The alignment was made using the program *ESPript* (Gouet *et al.*, 1999).

extended loop at residues 198–202. These elements from the two monomers enclose a large solvent cavity in which only part of the solvent is ordered in the current structure. The dimer interface is predominantly polar in nature, containing two sets of five salt bridges and a large number of direct or water-mediated hydrogen bonds. Three of the salt bridges have equivalents in all the bacterial structures, although with differences in participating residues. One salt bridge, between Asp85 and Arg307, is novel to the human structure. Asp85 is located on the loop connected to two helices that traverses the

synthetase domain from the nucleotide-binding domain. The corresponding loop in ecASS is extended and largely fills the solvent cavity found in the other structures. It is tempting to speculate that this domain-spanning structure could have long-range structural effects as a result of changes in the active site during the catalytic cycle.

3.3. Tetramer interface

The interface between the two dimers is primarily made up of helices 11 and 12 from the synthetase domains and helix 14 from the C-terminal oligomerization tail. Helices 11 and 12 from each monomer stack against their counterparts in the dimer neighbour, forming a mostly hydrophobic interface. The four pairs of helices surround an elongated solvent-filled cavity at the centre of the tetramer. The arrangement of helices is highly conserved between the human and bacterial structures, despite the only modest sequence identity in this area. The C-terminal tail of hASS is wedged between an identical tail from the neighbouring dimer and the nucleotide domain of its own dimer partner. This region closely aligns with the counterparts from ttASS and tmASS and many of the hydrophobic interactions are fully conserved in these structures. The C-terminal tail of ecASS is less similar to that of hASS and contains an additional two-stranded β-sheet at its extreme terminus. In hASS only one salt bridge can be found in the tetramer interface; it is between Arg398 on the C-terminal helix and Glu330 at the beginning of helix 12. This salt bridge is conserved in ttASS and tmASS, but not in ecASS.

3.4. Crystal contacts

The crystal lattice contains only one unique set of crystal contacts where neighbouring tetramers interact. This interface is made up of a helix and an extended loop spanning residues 159–175 on the nucleotide domain and a loop region at residues 205–218 on the synthetase domain. Possible effects of crystal contacts on enzyme function are discussed in §3.6.

3.5. Substrate binding

In the current structure of hASS, a citrulline molecule and an aspartate molecule have been built into the active site. The citrulline molecule is tightly anchored at the amino-acid moiety through salt bridges and hydrogen bonds to the side chains of Glu270, Tyr282, Arg127, Asn123 and Tyr87 (Fig. 2). Both N atoms of the ureido group are hydrogen bonded to the hydroxyl group of Ser189, while the O atom makes a hydrogen bond to the amine on the aspartate ligand. The aspartate carboxylate groups furthermore make hydrogen bonds to the backbone amines of Asn123 (side-chain carboxylate) and Thr119 (amino-acid carboxylate). The second oxygen of the

amino-acid carboxylate makes a hydrogen bond to the hydroxyl of Thr119. The binding modes of citrulline and aspartate in hASS do not differ significantly from those observed in bacterial structures with the same substrates present (1k97 for *E. coli* and 1j1z for *Tm. thermophilus*).

3.6. ATP

It has been shown that ecASS undergoes a conformational change upon binding of ATP that reduces the distance between the phosphates of ATP and the citrulline molecule (Lemke & Howell, 2002). The distance between the citrulline nucleophile and the α-phosphate of a modelled ATP molecule in the unbound form has been calculated as 7.9 Å. This distance is reduced to 5.8 Å in the liganded structure in which both ATP and citrulline are present. The binding involves a conformational change in which the nucleotide-binding domain approaches the synthetase domain in a hinge-like movement. In order for catalysis to take place the distance is believed to be reduced further and it has been suggested that rigidity arising from the crystal lattice hinders further closure of the gap.

In the ttASS–ATP–citrulline–aspartate complex the distance between the nucleophilic O atom on citrulline and the ATP α-phosphate is 4.8 Å, which is 1 Å shorter than that observed for the corresponding complex in ecASS. The conformational change seen in ecASS is not observed in ttASS and it is suggested that the citrulline molecule is repositioned towards ATP during the nucleophilic attack. This hypothesis is supported by the structure of the ttASS–ATP–argininosuccinate complex, in which the arginine moiety of the product is in close proximity to the ATP α-phosphate.
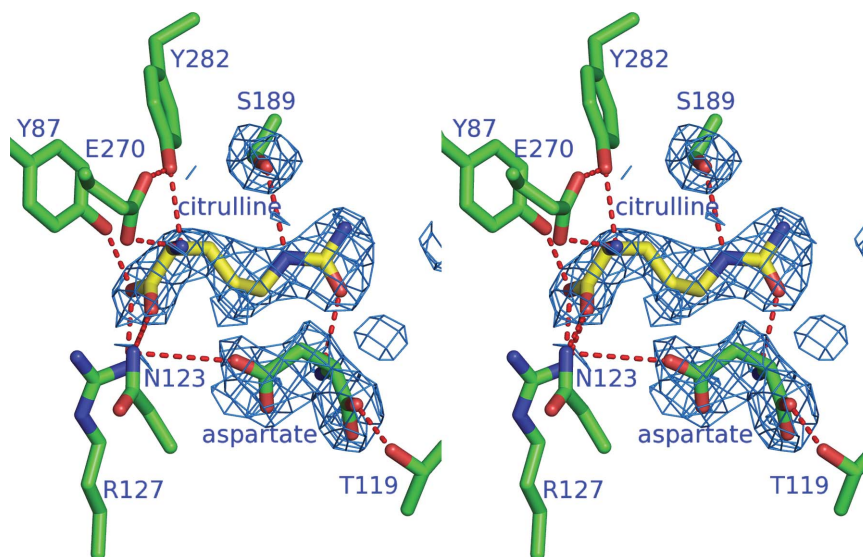

Figure 2
The substrates citrulline and aspartate modelled into the electron density. Human argininosuccinate synthetase (hASS) was cocrystallized with the two substrate molecules citrulline and aspartate. σ_A-weighted $2F_{obs} - F_{calc}$ density at 2.4 Å resolution is shown for these ligands. The ligand–protein interactions for hASS closely resemble those reported previously for bacterial structures. All figures were produced using *PyMOL* (DeLano, 2002).

In order to compare ATP binding between human and bacterial ASS, we have superposed an ATP molecule onto the current structure in order to obtain an estimate of the relative positions of the substrate molecules (Fig. 3). The distance between the citrulline nucleophilic O atom and the α-phosphate of the modelled ATP is 4.8 Å. This distance may be compared with a similar modelling performed for ecASS, in which the corresponding distance was found to be 7.9 Å. The large difference between these distances may indicate that a considerably smaller conformational change is needed for catalysis in hASS than that which has been demonstrated for ecASS. We have performed extensive crystallization and soaking trials with hASS in the presence of ATP. However, no X-ray quality crystals have been obtained. Since the current crystal form contains contacts between the nucleotide domain

Figure 3
Model of the interaction of ATP with substrate. An ATP molecule was modelled into the nucleotide-binding domain of human argininosuccinate synthetase using the homologous structure from *Th. thermophilus* (Goto *et al.*, 2003). The distance between the citrulline molecule and the ATP α-phosphate is shorter than the corresponding distance in the *E. coli* enzyme, in which a conformational change brings the two molecules closer upon ATP binding (Lemke & Howell, 2002).

and the synthetase domain of neighbouring tetramers, it may be prevented from forming properly if ATP binding causes a rearrangement of the two domains.

3.7. Nitrosylation

The amino acid that has been identified as the target of the regulatory nitrosylation by NOS in the human enzyme, Cys132 (Hao *et al.*, 2004), is found to be buried in the synthetase domain. The reversible nitrosylation of this residue fully inactivates the enzyme. Cys132 is conserved in mammalian ASS but not in those from plants or bacteria. It is not in direct contact with any of the substrates. The cysteine side chain points towards a cavity in the native structure (Fig. 4a). This cavity is surrounded by the side chains of Val114, Val141, Gln102, Phe128, Glu129 and His116; the polar moieties of Glu129 and His116 are pointing away from the pocket. The only polar feature of the pocket comes from the side chain of Gln102. Weak electron density for a solvent molecule can be found at the extension of this side chain. In order to estimate the effect of nitrosylation of Cys132, we aligned it with existing structures of nitrosylated cysteines (Fig. 4b). This alignment showed a common orientation of the added N atom in the published structures. If this conformation is predictive of the modified Cys132 in hASS, it would cause close contacts with the side chains of Val103 and Val114 and would require the repositioning of either these residues or Cys132 itself. A potential new polar interaction can also be seen between the nitrous N atom and the main-chain carbonyl O atom of Phe128.

The effect of nitrosylation on enzyme activity is hard to predict, since the distance between Cys132 and the active site is considerable. However, it should be noted that the residues likely to be perturbed are located on secondary-structure elements that are part of the active site. Even small conformational changes could therefore be propagated and influence catalytic properties. Interestingly, Hao *et al.* (2004) have shown that binding of ATP competitively protects the enzyme from nitrosylation. ATP is also the substrate molecule closest to Cys132, with a shortest distance of 10.1 Å between the cysteine S atom and a pentose hydroxyl. The side chain of Phe128 is of special interest, since it lies within van der Waals distance of the modelled ATP pentose ring. A small perturbation of this side chain upon ATP binding could rearrange the environment around the cysteine and affect the propensity for nitrosylation.

To date, there are only a few crystal structures available that contain nitrosylated cysteines. A common feature is a cysteine residue that is located close to the surface, although often pointing into the core protein. This would allow easy access to an external enzyme, yet produce a significant conformational change in the modified protein. In thioredoxin the modification of two nearby cysteine residues causes a small shift of the helix in which they are located (Weichsel *et al.*, 2007). In human haemoglobin the structural effect is more pronounced, with a large change in the tertiary structure of the complex (Chan *et al.*, 1998). The nitrosylation site in hASS differs from
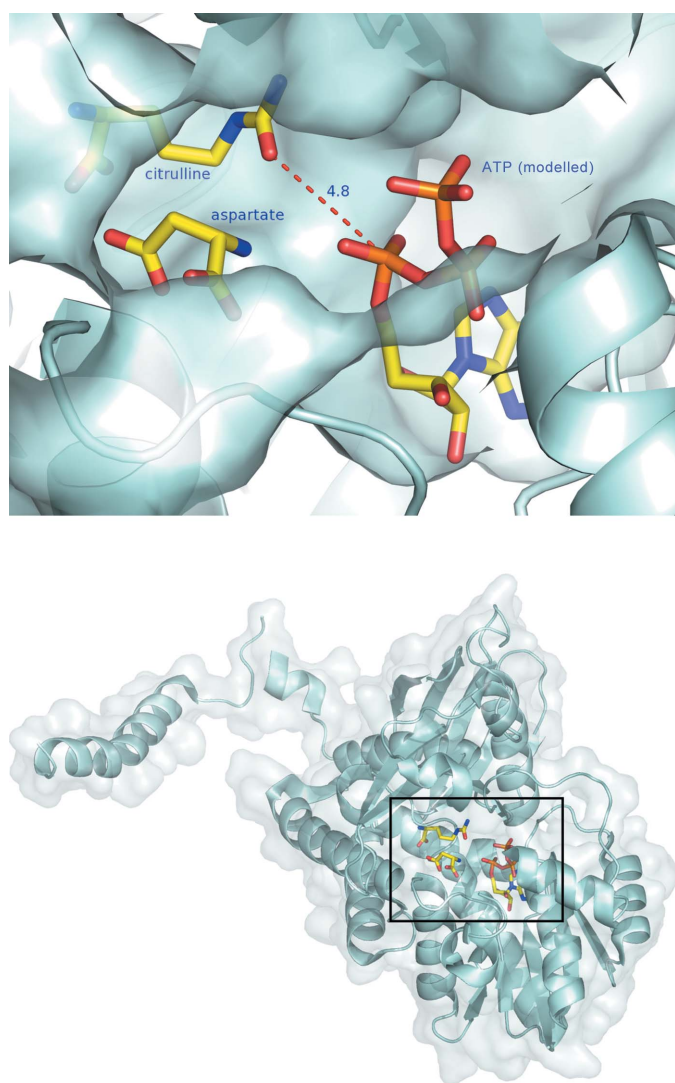
the available structures by being more deeply buried in the protein core and this suggests that a significant structural change is necessary for modification to occur.

3.8. Clinical mutations

A number of mutations have been identified in the human ASS gene, typically by the screening of patients and families diagnosed with citrullinaemia (Gao *et al.*, 2003; Häberle *et al.*, 2003). Many of these mutations have been mapped onto the structure of ASS using the bacterial structures as a template for the human structure (Lemke & Howell, 2001; Gao *et al.*, 2003). The current structure and its tetrameric complex confirm the majority of predictions made from these studies.
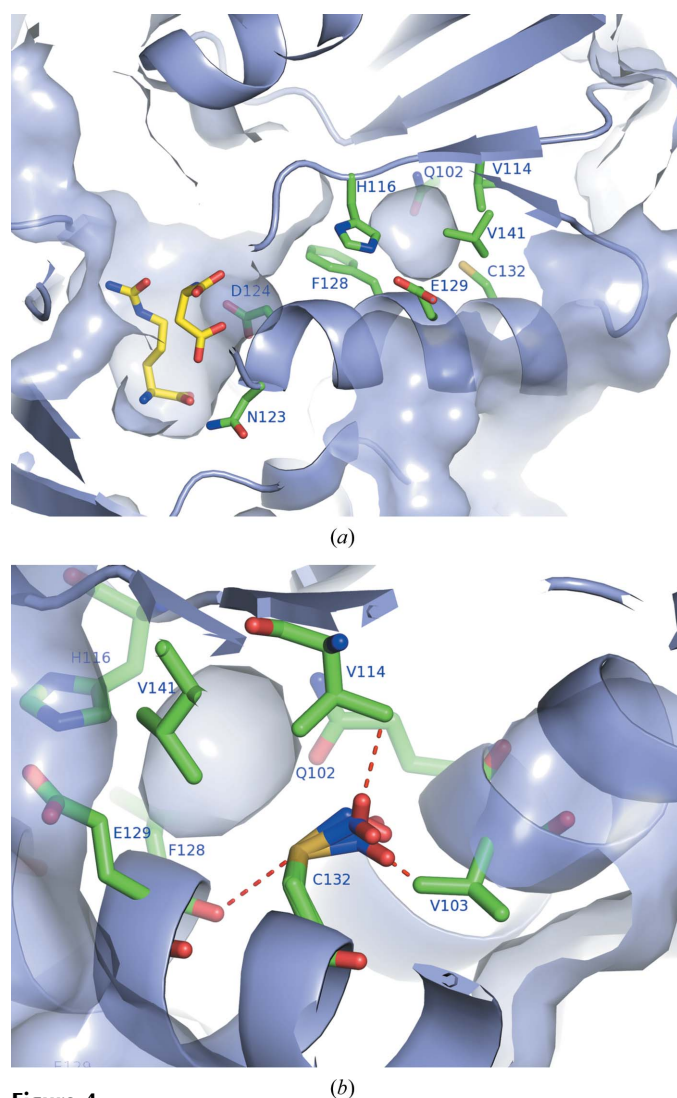

(a)

(b)

Figure 4
Cys132 and nitrosylation. The side chain of Cys132 is nitrosylated by nitric oxide synthase (NOS) as a down-regulating feedback mechanism (Hao *et al.*, 2004). NOS and argininosuccinate synthetase belong to the same pathway, the arginine–citrulline cycle. (*a*) In the nonnitrosylated structure of human ASS, the cysteine side chain is not located in the immediate vicinity of the active site. A small cavity, here shown as a van der Waals surface, is found next to the side-chain sulfur. (*b*) A group of nitrosylated cysteine residues found on proteins in the Protein Data Bank have been superimposed with Cys132.

For some of the mutated positions the human structure adds new detail and will be described here, with the mutation noted in parenthesis. Arg86(His) forms a salt bridge with Asp296 of a neighbouring monomer at the dimer interface. The shorter histidine side chain could decrease the strength of the salt bridge and potentially disturb the integrity of the dimer. The side chain of Arg265(His) is positioned to make a π–π hydrogen-bond interaction with the aromatic group of Tyr207. This interaction is likely to be lost in the mutant, although the effect on enzyme function is hard to predict, since the mutation is located at the surface and is not part of an oligomerization interface. Val269(Met) forms part of a hydrophobic cluster at the dimer interface together with Phe300 and Tyr370 from the neighbouring monomer. The much bulkier methionine side chain will push into the dimer partner and require a conformational change that could affect the stability of the complex. Lys310(Gln) points into the protein core, making a salt bridge with Glu298. This residue is located on a helix involved in dimerization, which could be disturbed by conformational changes and redistribution of charge caused by the mutation. The mutations described above are located far from the active site and they have all been classified as producing mild or asymptomatic phenotypes in patients (Gao *et al.*, 2003). Arg108(Leu) is a surface residue on the ATP-binding domain and forms weak (>4 Å) charge interactions with three surrounding glutamates: Glu62, Glu104 and Glu109. Although not in direct proximity to the active site, this nonconservative mutation has been observed in a patient with classical citrullinaemia (Häberle *et al.*, 2003).

Additionally, a number of novel mutations found in patients with mild citrullinaemia have recently been described by Häberle *et al.* (2003). Two mutations, Gln40(Leu) and Arg127(Gln), are directly involved in substrate binding and are likely to have a direct effect on catalytic efficiency. Gln40(Leu) is found in a loop between strand 2 and helix 2 and makes a hydrogen bond to the adenine group of ATP. Arg127(Gln) forms a salt bridge with the carboxylate group of citrulline. Ala202(Glu) is located on the surface, pointing into a hydrophobic cluster in the vicinity of the dimerization domain. The introduction of a glutamic acid could significantly disturb the secondary structure of this region and thereby affect dimerization. A similarly disruptive effect is possible for Arg307(Cys), which forms a salt bridge with Asp85 from a neighbouring molecule at the dimerization interface. Val345(Gly) is part of the synthetase-domain core structure at the beginning of a β-strand. This mutation could increase the flexibility and destabilize the structure in a region close to the dimerization interface. A mutation was also found that terminates the protein at residue 259. This protein would lack many of the citrulline interactions as well as most of the oligomerization framework and is unlikely to be properly folded.

4. Conclusions

The proper functioning of hASS is crucial for nitrogen homeostasis in the body, as evidenced by the many debilitating

mutations found in the ASS gene. The structure of hASS provides detailed insights into the nature of these mutations and how they affect the proper function of the enzyme. Nitrosylation of a cysteine residue is a key feature in the regulation of mammalian ASS. By modelling a nitroso group on Cys132, we obtain a first hint of the conformational changes that may take place as a consequence and how they could affect the catalytic activity. The structure includes two of the substrates, aspartate and citrulline, which are positioned in a manner similar to that seen in the bacterial structures, next to each other in the active-site pocket. The third substrate, ATP, could be modelled in its binding site; compared with the *E. coli* enzyme the position of the α-phosphate on ATP is closer to the carbonyl O atom on citrulline. This suggests a smaller conformational change upon catalysis for the human enzyme compared with the bacterial enzyme, in which the carbonyl O atom on citrulline makes a nucleophilic attack on the α-phosphate on ATP, producing the citrullyl-AMP intermediate. With the solution of the structure of human ASS, all the three-dimensional structures of the human enzymes of the urea pathway have now been described.

References

Chan, N. L., Rogers, P. H. & Arnone, A. (1998). *Biochemistry*, **37**, 16459–16464.

DeLano, W. L. (2002). *The PyMOL User's Manual*. DeLano Scientific, San Carlos, USA.

Emsley, P. & Cowtan, K. (2004). *Acta Cryst.* D**60**, 2126–2132.

Engh, R. A. & Huber, R. (1991). *Acta Cryst.* A**47**, 392–400.

Gao, H. Z. *et al.* (2003). *Hum. Mutat.* **22**, 24–34.

Goto, M., Nakajima, Y. & Hirotsu, K. (2002). *J. Biol. Chem.* **277**, 15890–15896.

Goto, M., Omi, R., Miyahara, I., Sugahara, M. & Hirotsu, K. (2003). *J. Biol. Chem.* **278**, 22964–22971.

Gouet, P., Courcelle, E., Stuart, D. I. & Metoz, F. (1999). *Bioinformatics*, **15**, 305–308.

Häberle, J., Pauli, S., Schmidt, E., Schulze-Eilfing, B., Berning, C. & Koch, H. G. (2003). *Mol. Genet. Metab.* **80**, 302–306.

Hao, G., Xie, L. & Gross, S. S. (2004). *J. Biol. Chem.* **279**, 36192–36200.

Husson, A., Brasse-Lagnel, C., Fairand, A., Renouf, S. & Lavoinne, A. (2003). *Eur. J. Biochem.* **270**, 1887–1899.

Kabsch, W. (1993). *J. Appl. Cryst.* **26**, 795–800.

Kleywegt, G. J. (1999). *Acta Cryst.* D**55**, 1878–1884.

Laskowski, R. A., MacArthur, M. W., Moss, D. S. & Thornton, J. M. (1993). *J. Appl. Cryst.* **26**, 283–291.

Lemke, C. T. & Howell, P. L. (2001). *Structure*, **9**, 1153–1164.

Lemke, C. T. & Howell, P. L. (2002). *J. Biol. Chem.* **277**, 13074–13081.

McMurray, W. C., Mohyuddin, F., Rossiter, R. J., Rathbun, J. C., Valentine, G. H., Goegler, S. J. & Zarfas, D. E. (1962). *Lancet*, **1**, 138.

Mori, M. & Gotoh, T. (2000). *Biochem. Biophys. Res. Commun.* **275**, 715–719.

Murshudov, G. N., Vagin, A. A. & Dodson, E. J. (1997). *Acta Cryst.* D**53**, 240–255.

Page, R., Grzechnik, S. K., Canaves, J. M., Spraggon, G., Kreusch, A., Kuhn, P., Stevens, R. C. & Lesley, S. A. (2003). *Acta Cryst.* D**59**, 1028–1037.

Ratner, S. & Petrack, B. (1951). *J. Biol. Chem.* **191**, 693–705.

Schimke, R. T. (1964). *J. Biol. Chem.* **230**, 136–145.

Schreiter, E. R., Rodríguez, M. M., Weichsel, A., Montfort, W. R. & Bonaventura, J. (2007). *J. Biol. Chem.* **282**, 19773–19780.

Vagin, A. & Teplyakov, A. (1997). *J. Appl. Cryst.* **30**, 1022–1025.

Weichsel, A., Brailey, J. L. & Montfort, W. R. (2007). *Biochemistry*, **46**, 1219–1227.